PHYSICAL REVIEW A **93**, 023823 (2016)

Time-to-frequency mapping of optical pulses using accelerating quasi-phase-matching

Mor Konsens and Alon Bahabad*

Department of Physical Electronics, School of Electrical Engineering, Fleischman Faculty of Engineering, Tel-Aviv University, Tel-Aviv 69978, Israel

(Received 16 October 2015; published 18 February 2016)

It is shown theoretically that the temporal profile of an optical pulse can be mapped to the spectral profile of its up-converted harmonic when an accelerating quasi-phase-matching modulation is used. Thus the problem of temporal measurement at a given frequency band is converted to the problem of spectral measurement at another frequency band. These results are developed and numerically demonstrated for the case of second-harmonic generation.

DOI: 10.1103/PhysRevA.93.023823

I. INTRODUCTION

Pulse characterization is an important problem in ultrafast optics to which there are various solutions based on nonlinear optics [1]. The most famous and commercially available are frequency-resolved optical gating (FROG) [2] and spectral phase interferometry for direct electric field reconstruction (SPIDER) [3]. Methods for direct time-to-frequency mapping of the amplitude of pulses are also known. These are based on the time-frequency duality between first-order dispersion and quadratic phase modulation and allow to estimate the intensity profile of pulses using spectral measurement after modulation of the original pulse [4–11]. Here we show that direct time to frequency mapping can be achieved by frequency converting an optical pulse to another frequency band following an interaction with a nonlinear spatiotemporal photonic crystal [12].

Efficient nonlinear optical frequency conversion requires compensation for phase mismatch caused by dispersion. Spatial quasi-phase-matching (QPM) modulation can be used to compensate for momentum mismatch and accomplish phase matching in energy-conserving nonlinear optical processes [13,14]. More generally, temporal QPM can accommodate a mismatch in energy while momentum is conserved, while spatiotemporal QPM can recompense for both momentum and energy mismatch [12]. Spatiotemporal QPM was realized using an all-optical modulation to enhance the efficiency of high-order-harmonic generation (HHG) [15]. In that work, a sequence of counterpropagating pulses interacted with a pump pulse to generate a QPM geometry described by a grating moving at a constant velocity (see discussion in Ref. [12]). The use of all-optical QPM suggests that spatiotemporal modulations, which are more involved than the steady moving grating, can be employed. For example, it is well known that two (quasi-cw) counterpropagating fields of different wavelengths would interfere to produce an intensity pattern which moves at a constant velocity (in contrast to a standing wave which is due to the interference of fields with the same wavelength). If at least one of these fields had a time-dependent wavelength (e.g., simple chirp), then the overall intensity pattern would necessarily move with a time-dependent velocity—it would accelerate. Yet, a more general form of an all-optical accelerating grating is technically possible: a modulation consisting (apart from the regular linear terms associated with the carrier frequency) of a sum of spatiotemporal bilinear terms (z^2, zt, t^2). It is possible to generate a field containing such terms by using prisms or gratings. In particular, spatiotemporal coupling is achievable through pulse front tilt (see a detailed review in Ref. [16]). In these cases, the spatial coordinate under consideration is transverse to the propagation direction. To induce a general bilinear spatiotemporal intensity pattern for the propagation coordinate for some pump pulse, two such spatiotemporal pulses can be used, propagating at a relative angle to each other (see Fig. 1).

The parameters of the modulation depend on the amount of initial chirp in each pulse, the amount of pulse front tilt, and the relative angle between the beams and the pump pulse. When the QPM modulation accelerates, light passing through the nonlinear material at different times would be subjected to different phase-matching conditions, allowing one to manipulate nonlinear frequency-conversion processes and shape the temporal and spectral profiles of the generated fields [17]. This basic idea is used here to show that an accelerating QPM modulation can facilitate time-to-frequency mapping of optical pulses. A judicious selection of the QPM geometry yields a spectrum which approximates the temporal intensity profile of the input pulse, while prior knowledge of the dispersion properties of the medium allows one to extract the exact profile. For simplicity, we develop this concept for second-harmonic generation. However, it should be adequate using an all-optical modulation of the nonlinear polarization for both HHG, where such a modulation was proven experimentally [15], and for perturbative frequency conversion in nonlinear crystals, as was suggested theoretically [18] and demonstrated recently [19].

II. THEORY

We start our theoretical treatment with the one-dimensional wave equation in the frequency domain for the second-harmonic (SH) electric field $\tilde{E}_{2\omega_0}(z,\omega)$ in a nonmagnetic medium under the nondepletion approximation:

$$\frac{\partial^2 \tilde{E}_{2\omega_0}(z,\omega)}{\partial z^2} + \beta^2(\omega)\tilde{E}_{2\omega_0}(z,\omega) = -\mu_0\omega^2\tilde{P}_{NL}(z,\omega), \quad (1)$$

where $\beta(\omega) = \frac{n(\omega)\omega}{c}$, $n(\omega)$ is the index of refraction, and $c = \frac{1}{\sqrt{\mu_0\varepsilon_0}}$ is the speed of light with μ_0 and ε_0 being the

*alonb@eng.tau.ac.il

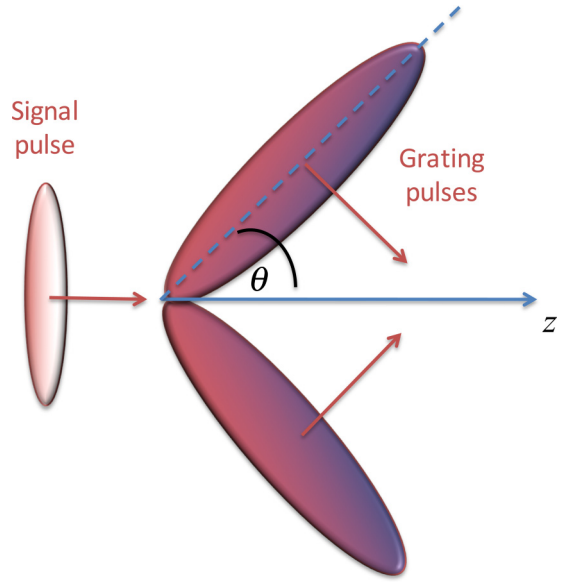

FIG. 1. General scheme for all-optical accelerating QPM. The grating pulses possess both temporal and transverse spatial chirp allowing the creation of the required spatiotemporal modulation along the z axis. The grating acts upon the signal (pump) pulse during the frequency-conversion process.

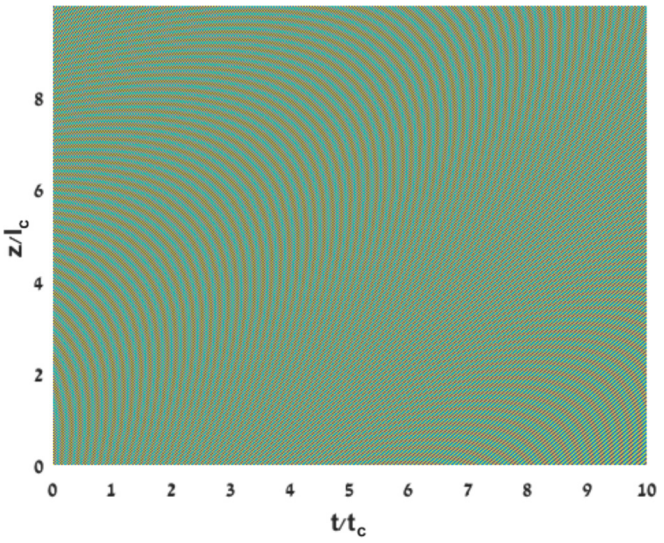

FIG. 2. Space-time diagram of the real part of an example of accelerating spatiotemporal QPM modulation. It can be seen that constant phase lines are curved in space-time, implying acceleration.

vacuum permeability and permittivity, respectively. $\tilde{P}_{NL}(z,\omega)$ is the Fourier transform of the material second-order nonlinear polarization,

$$P_{NL}(z,t) = \varepsilon_0 \chi^{(2)} g(z,t) E_{\omega_0}(z,t)^2, \tag{2}$$

where $\chi^{(2)}$ is the second-order electric susceptibility, $E_{\omega_0}(z,t)$ is the fundamental-harmonic (FH) electric field, and $g(z,t) = e^{i\Phi(z,t)}$ describes the QPM spatiotemporal geometry which macroscopically modulates the nonlinear polarization. The spatial (temporal) frequency of $\Phi(z,t)$ can be used to phase match a momentum (energy) mismatch of the nonlinear process [12]. In order to obtain a linear mapping from the time domain to the frequency domain, the modulation has to be such that the energy mismatch is a linear function of the reduced time τ in the frame moving at the FH pulse group velocity v_{g_1}: $\tau = t - \frac{z}{v_{g_1}}$, $\xi = z$. To find the phase function $\Phi(z,t)$ obeying this condition, we use the generalized phase-mismatch condition that exists between the energy mismatch $\Delta\omega$, the momentum mismatch Δk, and the material dispersion [12]:

$$\Delta k(\tau) = \Delta\omega(\tau)\frac{n(\omega_{SH})}{c} + \frac{2\omega_0}{c}[n(\omega_0) - n(\omega_{SH})], \tag{3}$$

where $\omega_{SH} = 2\omega_0 - \Delta\omega(\tau)$. To achieve phase matching, the instantaneous spatial and temporal frequencies of the phase function must obey $\frac{\partial\Phi}{dz} = \Delta k$ and $\frac{\partial\Phi}{dt} = -\Delta\omega$. In the τ, ξ frame,

$$\frac{\partial\Phi(\xi,\tau)}{\partial\xi} = \Delta k(\tau) - \frac{1}{v_{g_1}}\Delta\omega(\tau), \tag{4}$$

$$\frac{\partial\Phi(\xi,\tau)}{\partial\tau} = -\Delta\omega(\tau). \tag{5}$$

When group velocity dispersion can be neglected such that $v_{g1} = v_{g2}$, we can approximate

$$n(\omega_{SH}) = \frac{\frac{c}{v_{g_1}}\Delta\omega - 2\omega_0 n(2\omega_0)}{\Delta\omega - 2\omega_0}. \tag{6}$$

In this case, Eq. (4) is equal to the constant $\frac{2\omega_0}{c}[n(2\omega_0) - n(\omega_0)] \equiv -\Delta k_0$ and $|\Delta k_0| = \frac{\pi}{l_c}$, where l_c is the coherence length in an energy-conserving second-harmonic generation (SHG) process. With this approximation, any form of $\Delta\omega(\tau)$ can satisfy Eqs. (4) and (5). In particular, we can now choose the linear mapping, $\Delta\omega(\tau) = a + b\tau$, for which the solution of Eqs. (4) and (5) yields

$$\Phi(\xi,\tau) = -\Delta k_0 \xi - a\tau - \tfrac{1}{2}b\tau^2 + A_0, \tag{7}$$

where A_0 is an arbitrary constant. Notice that a change in the relative delay between the QPM modulation and the pump pulse translates to a change in the a and b parameters. Figure 2 depicts the space-time diagram of the real part of the accelerating spatiotemporal QPM modulation $g(z,t)$ with the phase function given by Eq. (7) for $b = \frac{\pi}{t_c^2}$, where $t_c = \frac{\pi}{|\Delta\omega_0|}$ is the coherence time in a momentum-conserving SHG process that corresponds to energy mismatch of $\Delta\omega_0 = \frac{2\omega_0}{n(2\omega_0 - \Delta\omega_0)}[n(2\omega_0 - \Delta\omega_0) - n(\omega_0)]$. For this figure, we set $A_0 = 0$ and $a = -bt_0$, with t_0 being at the middle of the FH pulse at $z = 0$, to achieve the central frequency of the SH field at $2\omega_0$. This is the actual modulation used for simulation in Sec. III below.

In the undepleted-pump approximation, the fundamental electric field is

$$E_{\omega_0}(z,t) = A\left(t - \frac{z}{v_{g_1}}\right)e^{i(\omega_0 t - k_0 z)}, \tag{8}$$

where $k_0 = \frac{n(\omega_0)\omega_0}{c}$ and $A(t - \frac{z}{v_{g_1}})$ is the pulse envelope we are interested in imprinting upon the SH spectrum. We now represent the envelope function with a Fourier series multiplied

by a Gaussian window function which isolates one instance of the periodic arrangement:

$$A(t) = e^{-\frac{t^2}{T^2}} \sum_{n=-\infty}^{\infty} f_n e^{i\tilde{\omega}_n t}, \tag{9}$$

where $\tilde{\omega}_n = \frac{2\pi n}{\tilde{T}}$ with an arbitrarily large time period $\tilde{T}$, and f_n are the Fourier series coefficients for this periodic expansion of the envelope. For such a representation, we require that $\tilde{T} \gg T \gg \tau_0$, with τ_0 being the temporal width of the FH. Under these conditions, we can write the envelope as

$$A\left(t - \frac{z}{v_{g_1}}\right) \cong e^{-\frac{t^2}{T^2}} \sum_{n=-\infty}^{\infty} f_n e^{i\tilde{\omega}_n (t - \frac{z}{v_{g_1}})}. \tag{10}$$

Notice that T can be set as large as required so the Gaussian function need not be moved together with the Fourier components. Substituting the modulation phase function given by Eq. (7) and the FH electric field given by Eqs. (8) and (10) into Eq. (2), and applying a Fourier transform in the time domain, results in

$$\tilde{P}_{NL}(z,\omega) = \sum_{n=-\infty}^{\infty}\sum_{m=-\infty}^{\infty} \frac{\varepsilon_0 \chi^{(2)}}{\sqrt{\frac{4}{T^2} - ib}} f_n f_m \times e^{-i(-\Delta k_0 + 2k_0 + \frac{a+\tilde{\omega}_n+\tilde{\omega}_m}{v_{g_1}})z} e^{i\frac{1}{2}b\frac{z^2}{{v_{g_1}}^2}} e^{-\frac{(\Omega + b\frac{z}{v_{g_1}})^2}{\frac{8}{T^2} - 2ib}}, \tag{11}$$

where Ω is defined as $\Omega = \omega - 2\omega_0 - a - \tilde{\omega}_n - \tilde{\omega}_m$. By selecting T such that $\frac{8}{T^2} \ll 2b$, Eq. (11) becomes

$$\tilde{P}_{NL}(z,\omega) = \frac{\varepsilon_0 \chi^{(2)}}{\sqrt{-ib}} e^{-iK(\omega)z} \sum_{n=-\infty}^{\infty}\sum_{m=-\infty}^{\infty} f_n f_m e^{-\frac{\Omega^2}{\frac{8}{T^2} - 2ib}}, \tag{12}$$

where $K(\omega) = -\Delta k_0 + 2k_0 + \frac{\omega - 2\omega_0}{v_{g_1}}$. Let us examine the rightmost expression,

$$e^{-\frac{\Omega^2}{\frac{8}{T^2} - 2ib}} \approx e^{-\frac{(\omega - 2\omega_0 - a)^2}{\frac{8}{T^2} - 2ib}} e^{-i\frac{(\omega - 2\omega_0 - a)(\tilde{\omega}_n + \tilde{\omega}_m)}{b}} e^{-i\frac{(\tilde{\omega}_n + \tilde{\omega}_m)^2}{2b}}. \tag{13}$$

As the $\tilde{\omega}_n$ frequencies span the FH envelope, their largest absolute values would be bounded by $1/\tau_0$ (this means that the Fourier coefficients for larger $\tilde{\omega}_n$ would be negligible). On the other hand, $|2(\omega - 2\omega_0 - a)|$ is bounded by $|b\tau_0|$. This means that for $b\tau_0^2 \gg 1$, we can neglect the expression $e^{-i\frac{(\tilde{\omega}_n + \tilde{\omega}_m)^2}{2b}}$ and get

$$\tilde{P}_{NL}(z,\omega) = \frac{\varepsilon_0 \chi^{(2)}}{\sqrt{-ib}} e^{-i\frac{(\omega - 2\omega_0 - a)^2}{2b}} e^{-iK(\omega)z} \times \left[A\left(\frac{\omega - 2\omega_0 - a}{b}\right)\right]^2, \tag{14}$$

where $A(t)$ is the temporal envelope of the input pulse. Solving the wave equation given by Eq. (1) with the spectrum of the nonlinear polarization given by Eq. (14) and the initial conditions $\tilde{E}_{2\omega_0}(z=0,\omega) = \frac{\partial}{\partial z}\tilde{E}_{2\omega_0}(z=0,\omega) = 0$ yields

$$\tilde{E}_{2\omega_0}(z,\omega) = r(z,\omega)\left[A\left(\frac{\omega - 2\omega_0 - a}{b}\right)\right]^2, \tag{15}$$

where

$$r(z,\omega) = -\frac{\mu_0 \varepsilon_0 \chi^{(2)}}{\sqrt{-ib}} \frac{\omega^2}{K(\omega)^2 - \beta(\omega)^2} e^{-i\frac{(\omega - 2\omega_0 - a)^2}{2b}} \times \left\{-e^{-iK(\omega)z} + \cos[\beta(\omega)z] - i\frac{K(\omega)}{\beta(\omega)}\sin[\beta(\omega)z]\right\}. \tag{16}$$

These last two equations constitute the major result of this paper and show that indeed using an accelerating QPM, the temporal profile $A(t)$ is mapped to the spectral profile of the generated harmonic radiation. We remind the reader that the a and b parameters reflect the relative delay between the pump pulse and the QPM accelerating grating. Thus a change in this delay translates to both a change in the central frequency of the up-converted spectrum and to a change in its bandwidth (seen as a stretch factor here). The term $r(z,\omega)$ represents the distortions in the time-to-frequency mapping due to dispersion of the FH during the nonlinear interaction. Still, most importantly, knowledge of the medium's dispersion and the pump group velocity completely determines $r(z,\omega)$, which allows one to extract the original FH amplitude regardless of the interaction length. In addition, in most cases, for the relevant frequency range, the phase velocity and group velocity would be close and the phase mismatch would be orders of magnitude smaller than the FH wave vector, which would lead to $K(\omega)/\beta(\omega) \approx 1$. In this case, we can approximate the amplitude of Eq. (16) as

$$|r| \cong \frac{\mu_0 \varepsilon_0 \chi^{(2)}}{|\sqrt{b}|}\left|\mathrm{sinc}\left\{\frac{[K(\omega) - \beta(\omega)]z}{2}\right\}\frac{z\omega^2}{K(\omega) + \beta(\omega)}\right|. \tag{17}$$

From this expression, we can estimate the distance at which the distortions get significant as $\min_\omega\{2\pi/[K(\omega) - \beta(\omega)]\}$. This value depends on the bandwidth of the generated SH pulse; however, assuming this bandwidth would be wider than the FH bandwidth, we can express the limiting case as the following dispersion length: $l_D = \tau_0^2/|\beta_2|$, where $\beta_2 = \max\{\beta_2^{FH}, \beta_2^{SH}\}$ is the maximum group velocity dispersion (GVD) over the GVD of the SH and of the FH pulses. For interaction lengths which are smaller than the dispersion length, the SH spectrum would constitute a good approximation to the envelope function (as long as we also keep $b\tau_0^2 \gg 1$). An important point to consider is that due to the phase-matched conditions under which this interaction takes place, the SH field is being built up efficiently and so a long interaction length increases the generated SH signal strength. The condition $b\tau_0^2 \gg 1$ also means that any chirp present in the envelope $A(t)$ is much smaller than the chirp rate b of the QPM modulation and so can be neglected. In this case, to achieve Δt temporal resolution for the FH requires $b\Delta t$ resolution in the spectrum of the SH. Significant chirp in the envelope would smear the time-to-frequency mapping. One last remark regarding this condition is that it is rather standard in the context of time-to-frequency mapping and realizations of a time lens. The initial pulse duration (which depends on its dispersion) is always restricted with respect to the system chirp [5,20,21]. We would also like to note that in our derivation, we used the nondepletion approximation. If depletion becomes significant, it would degrade the time-to-frequency mapping as it depends

on the intensity of the pump pulse, leading to distortions in the pulse profile during the interaction.

III. NUMERICAL RESULTS

To demonstrate the time-to-frequency mapping in our proposed system, we performed numerical simulations for SHG within the accelerating nonlinear photonic crystal. For this purpose, we convert the second-order differential wave equation given by Eq. (1) to two first-order differential equations. First, we define

$$\tilde{E}_{2\omega_0}(z,\omega) = \hat{E}_{2\omega_0}(z,\omega)e^{j\beta(\omega)z} \tag{18}$$

and substitute to the wave equation to get

$$\frac{\partial^2 \hat{E}_{2\omega_0}(z,\omega)}{\partial z^2} + 2j\beta(\omega)\frac{\partial \hat{E}_{2\omega_0}(z,\omega)}{\partial z} = -\mu_0\omega^2 \tilde{P}_{NL}(z,\omega)e^{-j\beta(\omega)z}. \tag{19}$$

By defining

$$H(z,\omega) = \frac{\partial \hat{E}_{2\omega_0}(z,\omega)}{\partial z}e^{2j\beta(\omega)z}, \tag{20}$$

Eq. (19) can be rewritten as

$$\frac{\partial H(z,\omega)}{\partial z} = -\mu_0\omega^2 \tilde{P}_{NL}(z,\omega)e^{j\beta(\omega)z}, \tag{21}$$

and, according to Eqs. (18) and (20), we obtain

$$H(z,\omega) = \left[\frac{\partial \tilde{E}_{2\omega_0}(z,\omega)}{\partial z} - j\beta(\omega)\tilde{E}_{2\omega_0}(z,\omega)\right]e^{j\beta(\omega)z}. \tag{22}$$

We solved Eqs. (21) and (22) using the Runge-Kutta 4 (RK4) method. We chose, for the simulations, propagation of an FH pulse in barium borate (BBO) [22] crystal. Notice that we assume an all-optical QPM mechanism and so we could choose any material with a second-order susceptibility for our purpose (that is, no need for choosing, for example, a ferroelectric crystal where the QPM physical mechanism is usually electric field poling). For a 800 nm pump, the ratio between the dispersion length for the SH and coherence length is ∼34. The FH is a pulse of ∼0.5 ps duration with an asymmetric envelope. The envelope of the FH pulse and the envelope squared are shown in Fig. 3(a). The use of two accelerating QPM geometries is demonstrated for two different values of b while $a = -1.1bt_0$. Figure 3(b) shows the SH spectrum—as integrated numerically (solid blue line) and from the analytical approximation (dashed red line) for $b\tau_0^2 = 4$ (left column) and $b\tau_0^2 = 40$ (right column) at three different propagation distances: $z/l_D = 0.1$, $z/l_D = 1$, and $z/l_D = 2.5$ (top, middle, and bottom row, respectively). It is evident that although for a small $b\tau_0^2$ ratio there is no agreement between the analytical and numerical result, when the chirp rate of the QPM pattern satisfies the requirement of $b\tau_0^2 \gg 1$, the agreement is very good. We note that to support the case $b\tau_0^2 = 40$, the bandwidth of the spatiotemporal modulation is $b\tau_0 = 80$ THz which translates to $\Delta\lambda = 27$ nm. Such bandwidths are easily achievable with moderate-duration commercial femtosecond lasers. In Fig. 3(c), the SH spectrum divided by the $r(z,\omega)$ function is given at $z/l_D = 2.5$ for the two cases of accelerating QPM chirp rate. When $b\tau_0^2 \gg 1$,

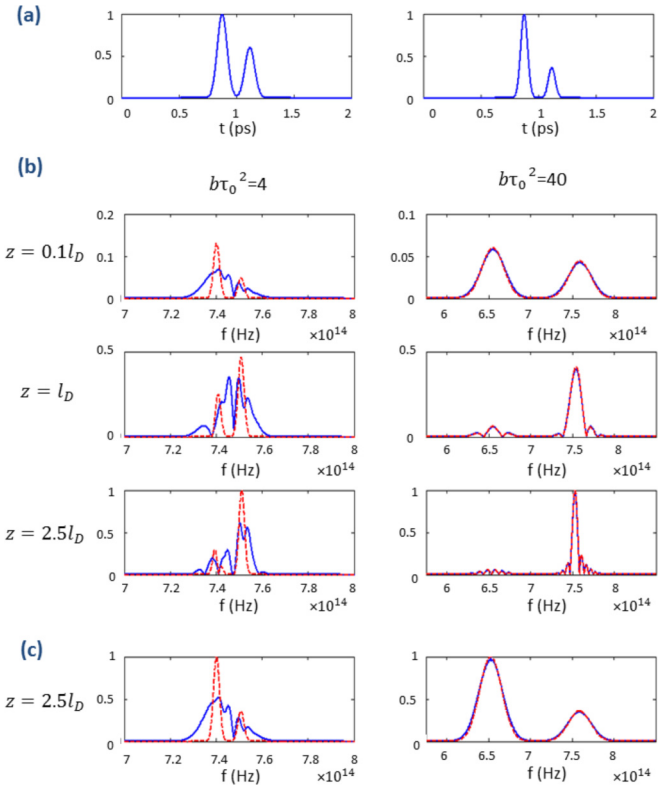

FIG. 3. Numerical and analytical results for the time-to-frequency mapping. (a) The temporal envelope of the FH pulse (left) and its square (right), (b) SH spectrum at three different propagation distances: $z/l_D = 0.1$, $z/l_D = 1$, and $z/l_d = 2.5$ (top, middle, and bottom row, respectively), and (c) the SH spectrum normalized by $r(z,\omega)$ at propagation distances of $z/l_D = 2.5$, where $b\tau_0^2 = 4$ (left column) and $b\tau_0^2 = 40$ (right column) as given by the numerical solution (solid blue line) and by the analytical expression (dashed red line). All amplitudes are in a.u.

the (squared) FH temporal envelope is clearly mapped to the spectrum of the SH. These results also demonstrate that for the case of $b\tau_0^2 \gg 1$, although the distortions are evident when the propagation is on the order of the dispersion length, the SH spectrum normalized by $r(z,\omega)$ at any value of z is an exact image of the square of the FH pulse waveform.

IV. CONCLUSIONS

To conclude, we have shown that accelerating quasi-phase-matching can be used for mapping optical pulses from the time domain to the frequency domain such that a temporal measurement can be replaced with a spectral measurement at a different frequency band than that of the original signal. Such a scheme might be useful for characterizing pulses whose spectral band suffers from lack of appropriate detectors. We analytically developed this scheme for the case of SHG with undepleted pump. However, the underlying principles can also be developed to other nonlinear frequency-conversion processes. Comparing our method with FROG [2], the need for synthesizing the spatiotemporal modulation makes it more complicated, while FROG also retrieves the phase of the original pulse. However, our method does have a few

advantages: when the dispersion of the nonlinear medium is known, the interaction length can be long, leading to better efficiency. In addition, it does not require a retrieval algorithm and it is single shot at one spatial dimension.

ACKNOWLEDGMENT

This work was supported by the Israeli Science Foundation, Grant No. 1233/13.

[1] I. A. Walmsley and C. Dorrer, Adv. Opt. Photon. **1**, 308 (2009).
[2] R. Trebino, *Frequency-Resolved Optical Gating: The Measurement of Ultrashort Laser Pulses: The Measurement of Ultrashort Laser Pulses*, Vol. 1 (Springer Science & Business Media, New York, 2000).
[3] C. Iaconis and I. A. Walmsley, Opt. Lett. **23**, 792 (1998).
[4] M. Vampouille, J. Marty, and C. Froehly, IEEE J. Quantum Electron. **22**, 192 (1986).
[5] M. Kauffman, W. Banyai, A. Godil, and D. Bloom, Appl. Phys. Lett. **64**, 270 (1994).
[6] L. K. Mouradian, F. Louradour, V. Messager, A. Barthélémy, and C. Froehly, IEEE J. Quantum Electron. **36**, 795 (2000).
[7] A. Galvanauskas, J. Tellefsen, Jr., A. Krotkus, M. Öberg, and B. Broberg, Appl. Phys. Lett. **60**, 145 (1992).
[8] Z. Jiang and X.-C. Zhang, Appl. Phys. Lett. **72**, 1945 (1998).
[9] T. Jannson, Opt. Lett. **8**, 232 (1983).
[10] J. Azaña and M. A. Muriel, IEEE J. Quantum Electron. **36**, 517 (2000).
[11] N. Berger, B. Levit, S. Atkins, and B. Fischer, Electron. Lett. **36**, 1644 (2000).
[12] A. Bahabad, M. M. Murnane, and H. C. Kapteyn, Nat. Photon. **4**, 570 (2010).
[13] R. W. Boyd, *Nonlinear Optics* (Academic, New York, 2003).
[14] J. Armstrong, N. Bloembergen, J. Ducuing, and P. Pershan, Phys. Rev. **127**, 1918 (1962).
[15] X. Zhang, A. L. Lytle, T. Popmintchev, X. Zhou, H. C. Kapteyn, M. M. Murnane, and O. Cohen, Nat. Phys. **3**, 270 (2007).
[16] S. Akturk, X. Gu, P. Bowlan, and R. Trebino, J. Opt. **12**, 093001 (2010).
[17] A. Bahabad, M. M. Murnane, and H. C. Kapteyn, Phys. Rev. A **84**, 033819 (2011).
[18] A. Bahabad, O. Cohen, M. Murnane, and H. Kapteyn, Opt. Express **16**, 15923 (2008).
[19] R. Myer, A. Penfield, E. Gagnon, and A. L. Lytle, in *Frontiers in Optics* (Optical Society of America, Washington, DC, USA, 2014), p. FTh4C.4.
[20] B. H. Kolner and M. Nazarathy, Opt. Lett. **14**, 630 (1989).
[21] M. A. Muriel, J. Azaña, and A. Carballar, Opt. Lett. **24**, 1 (1999).
[22] D. Eimerl, L. Davis, S. Velsko, E. Graham, and A. Zalkin, J. Appl. Phys. **62**, 1968 (1987).